10-1-2007

Ferrocene and Ferrocenium Modified Clays and Their Styrene and EVA Composites

Charles Manzi-Nshuti
Marquette University

Charles A. Wilkie
Marquette University, charles.wilkie@marquette.edu

Accepted version. *Polymer Degradation and Stability*, Vol. 92, No. 10 (October 2007): 1803-1812. DOI.

Ferrocene and Ferricenium Modified Clays and Their Styrene and EVA Composites

Charles Manzi-Nshuti
Department of Chemistry, Marquette University
Milwaukee, WI

Charles A. Wilkie
Department of Chemistry, Marquette University
Milwaukee, WI

Abstract:

In this work, ferrocene- and ferrocenium-containing salts were employed to modify montmorillonite. X-ray measurements show an increase in the interlayer spacing upon clay modification, which means that the larger and more organophilic cations were inserted into the gallery space of montmorillonite. Attempts to prepare nanocomposites of polystyrene and ethylene vinyl acetate copolymers lead to immiscible systems; the morphology of these systems was elucidated with TEM, XRD and cone calorimetry. The thermal stability of the composites is greater than that of the virgin polymer.

Keywords: Ferrocene, Polystyrene, Ethylene vinyl acetate copolymer, Nanocomposites.

Polymer Degradation and Stability, Vol. 92, No. 10 (October 2007): pg. 1803-1812. DOI.

1. Introduction

Polymer–clay nanocomposites have been studied extensively for several years, and it is now known that the fire properties, thermal stability [1] and [2], gas barrier properties [3], ionic conductivity [4], mechanical properties [5] and [6], etc., are all improved relative to the virgin polymer. Nanocomposites can be described as immiscible, intercalated or exfoliated depending on the type of dispersion of the nanomaterial in the polymer. In an immiscible system, also known as a microcomposite, the polymer does not enter into the gallery space of the nanomaterial and the nanomaterial acts as a filler in a conventional composite. An intercalated nanocomposite is obtained when the polymer enters the gallery space and the registry between the layers is maintained. In an exfoliated system, also referred to as a delaminated system, an excellent nano-dispersion of the layered material into the polymer matrix is accompanied with a loss of the registry between the layers. Wide-angle X-ray diffraction (XRD) and transmission electron microscopy (TEM) are the most commonly used methods to study the dispersion of the polymer matrix into the galleries of the inorganic material. Some of the properties of the nanocomposites, notably mechanical and permeability, are thought to be very dependant upon exfoliation while others, fire retardancy is the most notable, do not appear to show a difference between intercalated and exfoliated systems [7].

Because of the inorganic cations present in the galleries of the clay, clays are hydrophilic. To permit the entry of a polymer into the gallery space, the clay gallery space must become organophilic, which is usually accomplished by ion exchange with an organophilic ammonium ion [8] and [9] or other ions [10], [11] and [12]. Clays have an interlayer spacing which is much smaller than the radius of gyration of polymers. The distance between each pair of pristine clay layers is too small and will not easily allow the facile entry of monomer or polymer. In addition to enhancing the organophilicity of the gallery space, the surfactant also acts as a spacer, enlarging the interlayer spacing of the layered material to facilitate the entry of monomers or polymers into the gallery space.

Ferrocene-containing systems are a new type of surfactant with potentially promising properties. Ferrocene can undergo nucleophilic

Polymer Degradation and Stability, Vol. 92, No. 10 (October 2007): pg. 1803-1812. DOI.

aromatic substitution [13] and [14], like benzene, to allow the incorporation of long alkyl chains and it contains iron and thus the surfactant is both organic and inorganic. One of the simplest and most characteristic reactions of metallocenes is their oxidation to cationic species involving loss of an electron; ferrocene can be oxidized to the corresponding ferrocenium cation electrolytically, photolytically and by a wide variety of organic and inorganic oxidizing agents. When oxidized, a blue, relatively stable ferrocenium cation is formed [13]. The corresponding alkylferrocenium salts can then be used to modify clay to obtain a new organically modified clay which can then be used for nanocomposite formation. The expectation is that these ferrocenium-substituted clays will have better thermal stability than the typical ammonium-modified clay.

Another type of ferrocene-containing surfactants for clays has also been reported [15]: a series of ferrocenyl surfactants was tested as model compounds to study electron transfer reactions involving structural Fe(III) in the clay mineral. The surfactants contained trimethyl ammonium headgroups, ferrocene tail groups, and an intervening hydrocarbon spacer of 1, 6 or 11 carbons. It was shown that oxidation occurs in the last two where there is an intervening alkyl spacer of 6 or 11 carbon atoms, but no electron transfer occurred with only a single carbon atom as the spacer. In this study, similar surfactants were synthesized and used to modify sodium montmorillonite. One of the methyl groups in the trimethyl ammonium head group was replaced by a C_{12} or C_{16} tail, as it is known that the presence of a long alkyl chain can facilitate the incorporation of a polymer between the clay layers. The intent of this work is to design new surfactants, with enhanced thermal stability, and to prepare and evaluate the properties of their polymer nanocomposites.

2. Experimental

2.1. Materials

Most chemicals used in this study were purchased from Aldrich Chemical Company. Ferrocene, sodium hexafluorophosphate, palmitoyl chloride, myristoyl chloride, aluminum chloride, mercuric chloride, granular zinc (−30 + 100 mesh), dichloromethane, chloroform, benzene, hydrochloric acid, sulfuric acid, methanol, hexane, silica,

Polymer Degradation and Stability, Vol. 92, No. 10 (October 2007): pg. 1803-1812. DOI.

(dimethyaminomethyl)ferrocene, 1-bromohexadecane, lauryl bromide, acetone, styrene; inhibitor removers and polystyrene (Mn 140 000 and Mw 230 000). Ethylene vinyl acetate copolymer (EVA) with 19 wt% vinyl acetate was produced and kindly provided by ExxonMobil Co. Sodium montmorillonite, a cationic clay of composition $(Na_{0.35}K_{0.01}Ca_{0.02})$ $(Si_{3.89}Al_{0.11})(Al_{1.6}Fe_{0.08}$ $Mg_{0.32})O_{10}(OH)_2$, was provided by Southern Clay Products, Inc.

2.2. Synthesis of ferrocenyl ammonium salts

Two ferrocenyl surfactants were synthesized and used to modify sodium montmorillonite. Their synthesis followed a method reported by Saji et al. [16] with minor modification. The first surfactant was prepared as follows: equimolar amounts (0.02 mol) of ((dimethylamino)methyl)ferrocene and *n*-dodecyl bromide was stirred for 2 h at 60 °C. The reaction product was recrystallized twice from acetone to give a yellow-orange, crystalline product in a 60% yield. ^{1}H NMR 0.85 (t, 3H), 1.14–1.28 (m, 14H), 1.29–1.37(m, 4H), 1.71(s, 2H), 3.22 (s, 6H), 3.31(m, 2H), 4.27 (s, 5H), 4.30 (t, 2H), 4.48 (t, 2H), 4.87 (s, 2H).

The second surfactant was prepared following a similar procedure, but hexadecyl bromide was used instead of *n*-dodecyl bromide. A yellow, crystalline product, (72% yield) was obtained. ^{1}H NMR 0.85 (t, 3H), 1.14–1.26 (m, 22H), 1.27–1.36 (m, 4H), 1.68 (s, 2H), 3.22 (s, 6H), 3.31(m, 2H), 4.27 (s, 5H), 4.32 (t, 2H), 4.48 (t, 2H), 4.82 (s, 2H).

2.2.1. Modification of MMT

A 27 g portion of MMT was dispersed in 50:50 mixture of deionized water and methanol at 50 °C for 12 h. In another flask, 34 mmol of (ferrocenylmethyl)hexadecyldimethylammonium bromide was dissolved in a small amount of methanol, and this homogeneous solution was then added to the MMT solution and the stirring was continued for additional 20 h. The yellow precipitate was then washed with water and methanol and dried in a vacuum oven at 80 °C overnight to obtain the modified clay, designated as FERAC16. FERAC12 was obtained in a similar fashion from (ferrocenylmethyl)dodecyldimethylammonium bromide and MMT.

2.3. Synthesis of ferrocenium salts

It has been found that both acylferrocene and 1,1'-diacylferrocene can be prepared in a satisfactory yield by varying the ratio of ferrocene, acid chloride, and aluminum chloride, and the mode of addition [17]. Acylferrocenes are prepared by the dropwise addition of the acid chloride–aluminum chloride complex to the ferrocene solution, using equimolar amounts of the acid chloride, $AlCl_3$, and ferrocene. The disubstituted derivatives were prepared by adding the ferrocene solution to the acid chloride–$AlCl_3$ complex, using a molar ratio of both the acid chloride and the aluminum chloride to ferrocene of 4:3. The synthesis followed a literature procedure by Wang and Gokel [13], reagents being scaled up at least 10 times, with other minor modifications. Acylferrocenes and 1,1'-diacylferrocenes were prepared by Friedel–Crafts acylation and converted to the alkyl counterparts by the Clemmensen reduction.

2.3.1. Preparation of acylferrocenes

In a typical experiment, equimolar amounts (20 mmol) of the acid chloride and $AlCl_3$ in 100 ml of CH_2Cl_2 was added dropwise (2 h) to a solution of ferrocene (20 mmol in 100 ml of CH_2Cl_2) with stirring at room temperature. After 1 h, the reaction mixture was poured onto ice (200 g). The organic phase was washed with water until the washings were neutral and then dried over $MgSO_4$. After filtration, the solvent was evaporated, and the crude product was recrystallized twice from methanol to yield the final product. The 1-*n*-tetradecoylferrocene (65% yield) was obtained as an orange solid. ^{1}H NMR 0.88 (t, 3H), 1.26 (s, 20H), 1.71 (m, 2H), 2.69 (t, 2H), 4.20 (s, 5H, ferrocene), 4.49(t, 2H, ferrocene) 4.78 (t, 2H, ferrocene). 1-*n*-Hexadecoylferrocene (80% yield) was obtained as an orange solid by a similar procedure. ^{1}H NMR 0.88 (t, 3H), 1.26 (s, 24H), 1.71(m, 2H), 2.69 (t, 2H), 4.20 (s, 5H, ferrocene), 4.49 (t, 2H, ferrocene), 4.78 (t, 2H, ferrocene).

2.3.2. Preparation of 1-n-alkylferrocene

Granular zinc (50 g, 0.76 mol, 20 mesh) was amalgamated by stirring for 5 min with $HgCl_2$ (3.7 g, 0.014 mol), H_2O (73 ml) and concentrated HCl (ca 37%, v/v, 2.9 ml). The aqueous phase was

Polymer Degradation and Stability, Vol. 92, No. 10 (October 2007): pg. 1803-1812. DOI.

decanted and replaced by H_2O (88 ml), concentrated HCl (180 ml) and the acylferrocene (29 mmol), which was dissolved in benzene (60 ml). The mixture was heated at reflux for 55 h. At intervals during the reaction, (every 10 h), concentrated HCl (15 ml) was added. After the mixture was cooled to RT, the amalgam was removed and washed with diethyl ether. The combined organic phase was washed with water until neutral, and then dried over $MgSO_4$. The crude product was recrystallized from methanol. 1-*n*-Tetradecylferrocene was obtained as a yellow solid (75% yield). ^{1}H NMR: 0.88 (t, 3H), 1.26 (s, 22H), 1.49(m, 2H), 2.31 (t, 2H), 4.04–4.09 (three peaks, 9H, ferrocene). 1-*n*-Hexadecylferrocene, obtained by a similar procedure, was a yellow solid (70% yield). ^{1}H NMR: 0.88 (t, 3H), 1.26 (s, 26H), 1.49 (m, 2H), 2.31 (t, 2H), 4.04–4.09 (three peaks, 9H, ferrocene).

2.3.3. Preparation of 1,1′-bis(1-oxohexadecyl)ferrocene

Palmitoyl chloride (40 mmol) was slowly added to a suspension of $AlCl_3$ (40 mmol) in CH_2Cl_2 (150 ml) with stirring. To the above solution was added dropwise (2 h) a solution of ferrocene (30 mmol) in CH_2Cl_2 (200 ml) with stirring. After 12 h, the reaction mixture was poured onto ice (200 g). After adding $CHCl_3$ (150 ml), the organic phase was washed with water until neutral, dried over $MgSO_4$, and concentrated in vacuo. The product was purified by recrystallization twice from methanol. The product (orange-red solid) was obtained in a 60% yield. ^{1}H NMR: 0.88 (t, 6H), 1.26 (s, 48H), 1.69 (m, 4H), 2.65 (t, 4H), 4.48 (4H, ferrocene), 4.77 (t, 4H, ferrocene).

2.3.4. Preparation of 1,1′-bis(n-hexadecyl)ferrocene

Granular zinc (50 g, 0.76 mol, 20 mesh) was amalgamated by stirring for 5 min with mercury (II) chloride (3.7 g, 0.014 mmol), H_2O (74 ml) and concentrated HCl (2.9 ml). The aqueous phase was decanted and replaced by H_2O (88 ml), concentrated HCl (180 ml), toluene (100 ml) and the diacylferrocene (15 mmol). The mixture was heated at reflux for 55 h. At intervals during the reaction, (every 10 h), concentrated HCl (15 ml) was added. The amalgam was removed and washed with diethyl ether. The combined organic phase was washed with water until neutral and dried over $MgSO_4$. The crude product was chromatographed (silica, hexanes) to afford the product. 1,1′Bis(*n*-hexadecyl)ferrocene was a yellow solid (55% yield). ^{1}H NMR:

0.88 (t, 6H), 1.26 (s, 52H), 1.46(m, 4H), 2.21 (t, 4H), 4.10 (8H, ferrocene).

2.3.5. Preparation of the salt

Oxidation of mono (or bis) alkyferrocene compounds followed the literature procedure of Efendieya and Gasanov [18]. The reaction takes place at room temperature under an inert atmosphere (nitrogen). In a typical experiment, in a 200 ml flask under flowing nitrogen were placed 20 mmol of mono (or bis) alkylferrocene and 50 ml of concentrated sulfuric acid. The mixture was stirred for 1 h after which the yellow solution had turned blue. The solution was then diluted with deionized water (100 ml). In a separate flask, $NaPF_6$ (20 mmol) was dissolved in 50 ml of deionized water, and this solution was combined with the blue solution. The mixture was then stirred for an additional 10 min, and the blue precipitate was washed with deionized water and dried at room temperature. The salts were characterized by UV–vis spectroscopy (Table 1).

2.3.6. Modification of MMT

A 20 g portion of the sodium clay was dispersed in a 50:50 solution (water: THF) for 12 h. Mono (or bis)alkylferrocenium salt (23 mmol) was dissolved in a small amount of THF, and the two solutions were combined and stirred for an additional 48 h. The precipitate was then washed with water/THF until neutral and dried in a vacuum oven at 70 °C for 8 h to afford the ferrocenium clays (FERIC14, FERIC16 or BISFERIC16 where C14 and C16 are the length of the alkyl chain attached to the ferrocene group, and BIS means that there are two long chains attached on the surfactant).

2.4. Preparation of ferrocene/ferrocenium clay nanocomposites by melt blending

The nanocomposites were prepared by melt blending in a Brabender Plasticorder at high speed (60 rpm) at 190 °C for 20 min for PS and at 130 °C for 10 min for EVA. The composition of each nanocomposite is calculated from the amount of clay and polymer charged to the Brabender.

2.5. Instrumentation

^{1}H NMR spectra were obtained on a 300 MHZ Varian NMR spectrometer. UV–vis spectra were obtained on a Shimadzu UV-250IPC using dichloromethane as the solvent. X-ray diffraction (XRD) was performed on a Rigaku Geiger Flex, 2-circle powder diffractometer equipped with Cu Kα generator (λ = 1.5404 Å) at 50 kV and 20 mA, scanning from 0 to 10° at 0.1 step size. The samples were compression molded into 20 mm × 15 mm × 1 mm plaques for XRD measurements. Bright field transmission electron microscopy (TEM) images of the composites were obtained at 80 kV with a Zeiss 10c electron microscope. The samples were ultramicrotomed with a diamond knife on a Riechert–Jung Ultra-Cut E microtome at room temperature to give ~70 nm thick sections. These sections were transferred from a knife-edge to 600 hexagonal mesh Cu grids. The contrast between the layered silicates and the polymer phase was sufficient for imaging, so no heavy metal staining of sections prior to imaging is required. Thermogravimetric analysis (TGA) was performed on a SDT 2960 machine at the15 mg scale under a flowing nitrogen atmosphere at a scan rate of 20 °C/min. Temperatures are reproducible to ±3 °C, while the error on the fraction of non-volatile materials is ±2%. Cone calorimeter measurements were performed on an Atlas CONE-2 according to ASTM E 1352 at an incident flux of 35 kW/m^2 (PS) and 50 kW/m^2 (EVA) using a cone shaped heater; the exhaust flow was set at 24 L/s. The specimens for cone calorimetry were prepared by the compression molding of the sample (about 30 g) into 3 × 100 × 100 mm square plaques. Typical results from cone calorimetry are reproducible to within about ±10%; these uncertainties are based on many runs in which thousands of samples have been combusted [19].

3. Results and discussion

As noted above, the search for new, thermally stable, surfactants to modify clay for the preparation of nanocomposites has been a subject of extensive interest for some time. Two types of surfactants were synthesized in this study, one which contains a pendant ammonium ion on a ferrocene and the other contains a substituted ferrocenium cation. The syntheses of acylferrocene and 1,1'-diacylferrocene were carried out following the procedure of Wang

and Gokel [13]. Neutral ferrocene is yellow in solution while the positively charged ferrocenium is blue [15]. A color change after oxidation with sulfuric acid is an indication of the oxidation of ferrocene. As tabulated in Table 1, the oxidation of ferrocene was confirmed by UV–vis. The UV–vis spectra of the substituted ferrocene and its oxidized form in dichloromethane are shown in Fig. 1; the maximum absorbance is at 445 nm for tetradecylferrocene and moves to 636 nm upon oxidation to the ferrocenium salt. Similar UV–vis spectra were also obtained for FERIC16 and BISFERIC16. The structures of the cations are shown in Fig. 2.

3.1. XRD characterization of the organically modified clays

In Fig. 3 are shown the XRD traces of MMT and the ferrocene–ammonium-modified clays, FERAC12 and FERAC16. The basal spacing of MMT (2θ = 7.5) increases about 0.9 nm (2θ = 4.1) and 1.4 nm (2θ = 3.4), upon modification with FERAC12 and FERAC16, respectively. These results may indicate that the new surfactants are indeed intercalated inside the gallery space of the clay; the difference of 4 carbons between the two surfactants leads to an increase of about 0.5 nm, which may suggest that the alkyl chains are perpendicular to the layers following the calculations of Weiss [20], who calculated an increase of approximately 1.26 Å per carbon atom when the alkyl chains are perpendicular to the layers. This takes into consideration the angle formed by the sp^3 carbon and the length of a single C–C of 1.54 Å. Following his calculations, an increase of 5 Å is expected when the chain length of the long alkyl tail is increased by 4 carbon atoms.

Fig. 4 shows the XRD traces of MMT and the two ferrocenium modified clays, FERIC16 and BISFERIC16. With a vertical surfactant with a C16 chain, the interlayer distance would normally have to increase by about 2.0 nm. An increase of the basal spacing of 0.2 nm (2θ = 6.5) and 0.3 nm (2θ = 6.1), respectively, for FERIC16 and BISFERIC16 was observed. These XRD results may suggest a very low angle of tilt of the surfactants or at the extreme, a longitudinal arrangement with axes almost parallel to the silicate layers. This very large difference between the ferrocene–ammonium and the ferrocenium clays gives some possible indication of the arrangement of the cations and also suggests that there is a greater chance of

Polymer Degradation and Stability, Vol. 92, No. 10 (October 2007): pg. 1803-1812. DOI.

nanocomposite formation with the ferrocene–ammonium material than with the ferrocenium material.

3.2. Morphology of PS and EVA derivatives

Fig. 5 shows the X-ray traces of PS melt blended with different loadings of FERAC16 (the ferrocene–ammonium clay). Upon melt blending of FERAC16 and PS, a new peak appears at higher angles for all composites, indicating a decrease in the basal spacing. If the polymer enters into the gallery space of the clay, an increase in *d*-spacing is expected. The composites obtained after melt blending were dark green while the modified clay was yellow; there may be some interaction that occurs between the polymer and the clay or the clay may undergo some thermal degradation during processing. Attempts to produce PS nanocomposites by bulk polymerization using these ferrocene/ferrocenium clays failed because the clay could not be well-dispersed in the monomer. FERAC16 was also bulk polymerized with MMA and a similar observation was noted. TEM image (not provided) of the polymer obtained confirm the formation of a microcomposite. More work needs to be done to understand this finding.

From Fig. 6, one may suggest that upon melt blending, EVA and EVA/FERAC16 composites form immiscible systems. No new peak appears at low 2θ values, a sign of intercalation, but a new peak is seen at higher 2θ suggesting the formation of microcomposites.

3.3. Transmission electron microscopy (TEM)

The TEM image at low magnification is used to determine the dispersion of the clay in the polymer while the higher magnification image enables the description of the material as intercalated or exfoliated. Fig. 7 shows the low magnification images of the (left) EVA and (right) styrene systems of the (ferrocenylmethyl)hexadecyldimethylammonium-substituted clay (FERAC16). In both cases, one can see from the low magnification image that the clay is not well-dispersed. Fig. 8 shows the low magnification images of the styrene system of the tetradecylferrocenium-substituted clay (right) and the hexadecylferrocenium-substituted clay (left). In both cases, large tactoids are observed, suggesting poor dispersion of the clay in the

polymer matrix. If one assumes that these TEM images are representative of the bulk material, only microcomposites have been obtained in this study.

3.4. Thermogravimetric analysis

TGA enables the characterization of the degradation of the polymer [21]. Frequently the mass loss at 10% degradation, $T_{0.1}$, taken as the onset of the degradation and that at 50% degradation, $T_{0.5}$, along with the mass remaining at high temperature, char, are tabulated to describe the degradation.

3.4.1. Thermal stability of organically modified clays

After modification of sodium montmorillonite by either the ferrocene–ammonium or the ferrocenium salt, the clay is subjected to thermal degradation. A Hofmann elimination has been suggested to explain the two steps in the degradation of the typical ammonium clay [22] and [28]. In the first step, which occurs in the range of 200–400 °C, the long chain is lost as an olefin and a hydrogen replaces the alkyl group. In the second step, which commences at about 400 °C, the amine is lost and a proton is now the counterion for the clay. In Fig. 9, one can clearly see two steps in the degradation of FERAC16, while the second step is not very obvious for FERAC12. The first step occurs in the range of 150–250 °C and the second step in the range of 320–540 °C. The hexadecyl group is 48% of the total mass of the ferrocene ammonium cation and 16% of the modified clay. TGA curve shows only a 6% mass lost at 250 °C, so the complete loss of the olefin does not occur, unlike the case of the typical ammonium clays where degradation is complete. A similar observation is noted with FERAC12 where only 5% of the total clay mass is lost at 250 °C. If the dodecyl group was completely lost in the first step of degradation, the TGA would show a 12% mass loss in that step. It was also noted that the first step of degradation of FERAC12 commences early relative to FERAC16 (155 °C versus 190 °C). At 600 °C, if all surfactants were lost in the TGA experiment, it was estimated that a 30% mass loss should then be observed for FERAC16 and 27% for FERAC12. At this temperature, the mass loss is 21% for FERAC16, while a 13% mass loss at the same temperature was recorded for FERAC12. The remaining mass is greater than the expected mass, and this suggests that not all the surfactants were lost at 600 °C for these two clays.

Polymer Degradation and Stability, Vol. 92, No. 10 (October 2007): pg. 1803-1812. DOI.

Fig. 10 shows the TGA curves of two ferrocenium modified clays. FERIC16 degrades in two steps; at 250 °C, about 7% of the mass was lost, which does not account for complete loss of the hexadecyl group. At 250 °C, only 3% of the mass is lost for BISFERIC16 clay. This implies enhanced thermal stability for the bis-substituted ferrocenium clay. At 600 °C, FERIC16 and BISFERIC16 lose 25 and 37% of their total masses, respectively. These values are very close to the calculated values of 27 and 37% using a cation exchange capacity of MMT of 108 mequiv/100 g clay [23] and assuming the iron is left in the residue as the metal.

3.4.2. Thermal stability of the PS and EVA composites

The TGA results are presented in both tabular form, Table 2 and the actual TGA curves are shown in Fig. 11, Fig. 12, Fig. 13 and Fig. 14. The onset temperature is increased significantly as is the temperature at the mid-point of the degradation for PS. Of particular interest are the two systems, PS/FERIC16 and PS/BISFERIC16. It can be clearly seen that when two alkyl chains are present on the ferrocene (BISFERIC16 clay), the thermal stability of PS is greatly improved relative to when only one chain is present (FERIC16 clay). For example, at 1% loading of FERIC16 in PS, the onset temperature is 372 °C while at a same loading, a temperature of 381 °C is recorded for BISFERIC16. A similar observation is noted at 3% clay loading with the same polymer as can be observed in Table 2. These data reveal that when two long alkyl chains are present on the cation of the clay, the thermal stability of the composites is enhanced. Previous work from this laboratory suggested that the nano-dispersed clay changes the degradation pathway of polystyrene–clay nanocomposites, by confining the radicals formed during degradation, leading to radical recombination reactions which can account for the improvement in thermal stability relative to the pure polymer [24]. TEM and XRD of these systems suggested the formation of microcomposites. It was noted that the presence of the modified clays enhance the thermal stability of the polymer to various extents, with the more thermally stable BISFERIC16 giving more improvement compared to FERIC16.

The degradation of the EVA composites is shown in Fig. 14 which shows two degradation steps for all systems. In the first degradation step, all EVA/FERAC16 systems are less stable relative to

the pure polymer while the trends are reversed in the second step. The thermal degradation of EVA in nitrogen was reported by Camino et al. [25] as having two distinct regions, which were assigned to the loss of acetic acid and the degradation of the resulting unsaturated material, respectively. Work done previously in this laboratory [26] revealed that upon nanocomposite formation, the loss of acetic acid is accelerated as a function of clay loading, probably due to catalytic effect of the acidic sites of the clay. It was also shown that the stability of the nanocomposite is improved relative to virgin EVA when 50% mass loss is the point of comparison. In this particular case, an early degradation of the EVA composite with 3% clay relative to pure EVA is noted, and also an improvement in thermal stability at the mid-point temperature is observed. The expansion of the first step also provided in Fig. 14 shows that even a smaller amount of clay will affect the thermal stability of this polymer.

3.5. Fire performance of the polystyrene composites

The fire properties of PS and PS/FERIC14 composites were assessed by cone calorimetry; the parameters of interest are the time-to-ignition, which is usually smaller for nanocomposites than the virgin polymer, the peak of heat release rate (PHRR) and the percentage reduction in this value caused by nanocomposite formation, the total heat released, which is usually constant for polymers and their nanocomposites; and the mass loss rate. The change in the peak heat release rate is usually explained by the change in the mass loss rate. The results are tabulated in Table 3 and the heat release curves are shown in Fig. 15.

As can be seen in Table 3, the total heat released is constant for all systems, which indicates that the entire polymer burns. The rate of heat release from burning combustibles is usually considered as the most important in predicting the course of the fire and its effect [27]. The reduction in PHRR as recorded in Table 3 is much smaller than usually seen for PS nanocomposite (50–60%) [28] which also confirms that the polymer and the clay form immiscible systems. The time-to-ignition is shortened, as is usually seen for nanocomposites.

3.6. Fire performance of EVA composites

Fig. 16 shows the HRR curves of EVA and EVA/FERAC16 systems where a reduction in the peak heat release rate (PHRR) at this relatively small clay loading is noted; the complete results are provided in Table 4. At 1% clay loading, a 27% reduction in PHRR is obtained while 3% clay leads to a 33% reduction. For comparison, a reduction of 50–60% is seen with conventional organic modification [26]. The total heat released (THR) was virtually unchanged, which is the expectation for polymer–clay nanocomposites [19]. It is also noted that the presence of this clay doesn't increase the amount of smoke (ASEA) produced. Previous work on polymer nanocomposites has shown that there is essentially no reduction in PHRR for a microcomposite while there is a good reduction for any system which shows good nano-dispersion [19] and [29]. The results from EVA/FERAC16 are promising and suggest some interaction between the clay and this polymer as reduction is noted at a small clay loading. The TEM image suggests a microcomposite and the cone calorimetric results argue that some substantial portions of the clay are only micro-dispersed.

4. Conclusions

New ferrocenyl surfactants were synthesized and successfully used to modify sodium montmorillonite. The TGA of ferrocene–ammonium clays (FERAC12 and FERAC16) indicates two degradation steps, the first in the 155–200 °C range and the second at higher temperature. In the case of the ferrocenium clays, FERIC16 also degrades in two steps, with about 7% of the mass lost at 250 °C, which does not account for the complete lost of the hexadecyl group. At 250 °C, only 3% of the total mass is lost for BISFERIC16 clay, which implies a higher thermal stability for the disubstituted material. The composites are more thermally stable than the pure polymer. According to XRD and TEM, the modified clays are not well distributed throughout the PS and EVA polymer matrices; they are microcomposites. The reductions in PHRR recorded for PS/FERIC14 are much smaller than usually seen for PS nanocomposite (50–60%) which also confirms that the polymer and the clay form immiscible systems. Due to the poor dispersion of the clay in the polymer, these systems do not offer significant opportunity for enhanced properties

upon nanocomposite formation. Since the ferrocenium clays appear to be more thermally stable than the typical ammonium-substituted clays, if these can be obtained in a well-dispersed state; this may be an interesting system for further study. Work is currently underway to obtain better dispersion.

References

1. Zhu J, Wilkie CA. Polym Int 2000;49:1158-63.

2. Gilman JW, Kashiwagi T, Giannelis EP, Manias E, Lomakin S, Litchtenham JD, et al. In: Le Bras M, Camino G, Bourbigot S, Delobel R, editors. Fire retardancy of polymers: the use of intumescence. Cambridge, England: Royal Society of Chemistry; 1998. p. 201-21.

3. Lan T, Kaviratna PD, Pinnavaia TJ. Chem Mater 1994;6:573-5.

4. Vaia RA, Vasudevan S, Krawiec W, Scanlon LG, Giannelis EP. Adv Mater 1995;7:154-6.

5. Kojima Y, Usuki A, Kawasumi M, Okada A, Fukushima Y, Karauchi T, et al. J Mater Res 1993;8:1185-9.

6. Kojima Y, Usuki A, Kawasumi M, Okada A, Fukushima Y, Karauchi T, et al. J Polym Sci Part A Polym Chem 1993;31:983-6.

7. Su S, Jiang DD, Wilkie CA. Polym Adv Technol 2004;15:225-31.

8. Moet A, Akehah A. J Mater Sci 1996;31:3589.

9. Sue S, Wilkie CA. J Polym Sci Part A Polym Chem 2003;41:1124-35.

10. Wang D, Wilkie CA. Polym Degrad Stab 2003;82:309-15.

11. Zheng J, Wilkie CA. Polym Degrad Stab 2003;81:539-50.

12. Zhang J, Wilkie CA. Polym Degrad Stab 2004;83:301-7.

13. Wang K, Gokel GW. J Phys Org Chem 1997;10:323-34.

14. Vukicevic MD, Ratkovic ZR, Teodorovic AV, Stojanovic GS, Vukicevic RD. Tetrahedron 2002;58:9001-6.

15. Swearingen C, Wu J, Stucki J, Fitch A. Environ Sci Technol 2004;38:5598-603.

16. Saji T, Hoshino K, Aoyagui S. J Am Chem Soc 1985;107:6865-73.

17. Vogel M, Rausch M, Rosenberg H. J Org Chem 1957;22:1016-8.

18. Efendieva ZS, Gasanov TK. Azerbaidzhanskii Kwimicheskii Zhurnal 1985;4:83-5.

19. Gilman JW, Kashiwagi T, Nyden M, Brown JET, Jackson CL, Lomakin S, et al. In: AI-Malaika S, Golovoy A, Wilkie CA, editors. Chemistry and technology of polymer additives. Oxford: Blackwell Scientific; 1999. p. 249-65.

20. Weiss A. Angew Chem 1963;75:113-22.

21. Brown ME. Introduction to thermal analysis: techniques and applications; 1988. p. 7-21.

22. Xie W, Gao Z, Pan W-P, Vaia R, Hunter D, Singh A. Polym Mater Sci Eng 2000;83:284.

23. Leroux F, Besse J. Chem Mater 2001;13:3507-15.

24. Jang BN, Wilkie CA. Polymer 2005;46:2933-42.

25. Camino G, Sgobbi R, Colombier C, Scelza C. Fire Mater 2000;24:85.

26. Costache MC, Jiang DD, Wilkie CA. Polymer 2005;46:6947.

27. Babrauskas V. Fire Mater 1984;8:84-95.

28. Zhu J, Morgan AB, Lamelas FL, Wilkie CA. Chem Mater 2001;13:3774-80

29. Zhu J, Start P, Mauritz KA, Wilkie CA. Polym Degrad Stab 2002;77:253.

About the Authors

Charles A. Wilkie : Department of Chemistry, Marquette University, PO Box 1881, Milwaukee, WI 53201, United States

Email: charles.wilkie@marquette.edu

Appendix

Table 1: UV-vis λ_{Max} for ferrocenes and ferrocenium ions (CH_2CI_2)

	Ferrocene	Ferrocenium ion
	λ_{Max} (nm)	λ_{Max} (nm)
Ferrocene	443	624
Tetradecylferrocene	445	636
Hexadecylferrocene	443	623
Bis(hexadecyl)ferrocene	436	646

Table 2: TGA of different polymeric systems in this study

Composition	$T_{0.1}$ (°C)	$T_{0.5}$ (°C)
PS	346	408
PS/FERAC16 0.5%	396	426
PS/FERAC16 1%	397	427
PS/FERAC16 3%	409	431
PS/FERAC16 5%	413	436
PS/FERIC16 0.5%	367	415
PS/FERIC16 1%	372	418
PS/FERIC16 3%	384	423
PS/BISFERIC16 1%	381	422
PS/BISFERIC16 3%	395	429
PS/BISFERIC16 5%	418	429
EVA	362	472
EVA/FERAC16 0.5%	361	479
EVA/FERAC16 1%	360	479
EVA/FERAC16	351	482

Table 3: Cone summary results PS/FERIC14 (melt blended) at 35 kW/m^2

Formulation	PHRR (kW/m^2) (% Reduction)	THR (MJ/m^2)	ASEA (m^2/kg)	AMLR (g/s m^2)	t_{ign} (s)
PS	1480 ± 35	102 ± 0	1280 ± 23	34.1 ± 1.8	56 ± 1.5
PS/FERIC14 (0.5%)	1354 ± 88 (9)	99 ± 1	1264 ± 44	32.6 ± 1.4	56 ± 0.7
PS/FERIC14 (1%)	1313 ± 44 (11)	99 ± 1	1265 ± 19	31.9 ± 0.8	43 ± 6.0
PS/FERIC14 (3%)	1089 ± 11 (26)	97 ± 1	1290 ± 10	27.6 ± 0.1	35 ± 1.3
PS/FERIC14* (5%)	1045 ± NA (29)	96 ± NA	1293 ± NA	26.1 ± NA	37 ± NA

Polymer Degradation and Stability, Vol. 92, No. 10 (October 2007): pg. 1803-1812. DOI.

PHRR, peak heat release rate; THR, total heat released; ASEA, average specific extinction area (a measure of smoke produced); AMLR, average mass loss rate; t_{ign}, time-to-ignite.
* The PS/FERIC14 at 5% clay loading was run because not enough material was obtained after melt blending.

Table 4: Cone summary results EVA/FERAC16 at 50 kW/m^2

Formulation	PHRR (kW/m^2) (% reduction)	THR (MJ/m^2)	ASEA (m^2/kg)	AMLR (g/s m^2)	t_{ign} (s)
EVA	2450 ± 128 (NA)	109 ± 1	388 ± 6	29.1 ± 0.7	37 ± 0.1
EVA/FERAC16 (1%)	1790 ± 191 (27)	97 ± 4	377 ± 9	28.2 ± 1.5	35 ± 2.1
EVA/FERAC16 (3%)	1630 ± 96 (33)	102 ± 5	374 ± 15	29.6 ± 0.4	34 ± 1.7

PHRR, peak heat release rate; THR, total heat released; ASEA, average specific extinction area (a measure of smoke produced); AMLR, average mass loss rate; t_{ign}, time-to-ignite.

Fig. 1.: UV–vis spectrum of tetradecylferrocene and the corresponding ferrocenium salt in dichloromethane.

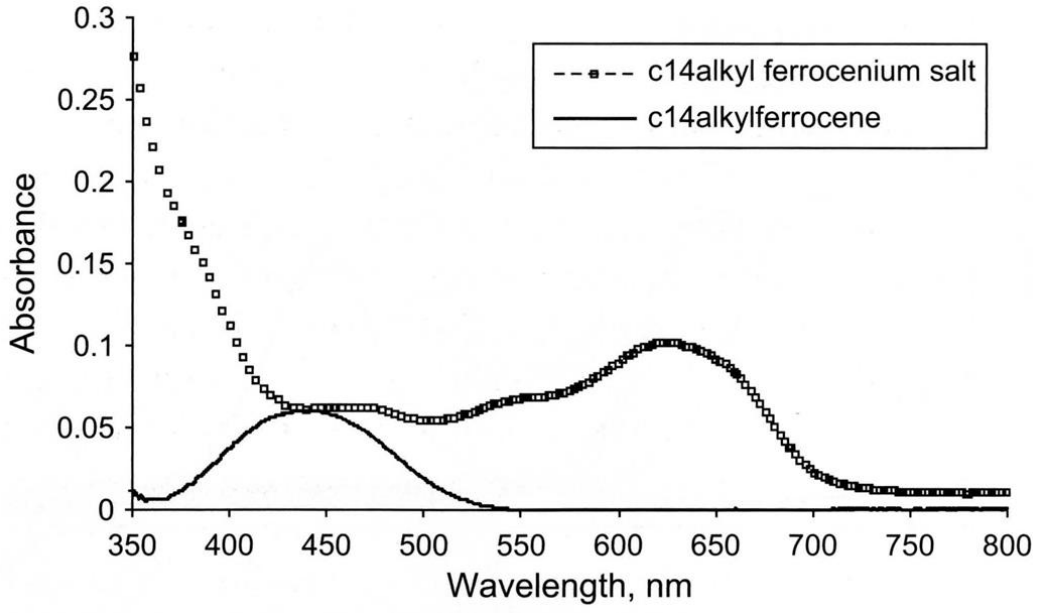

Polymer Degradation and Stability, Vol. 92, No. 10 (October 2007): pg. 1803-1812. DOI.

Fig. 2.: Structures of cationic surfactants used in this study.

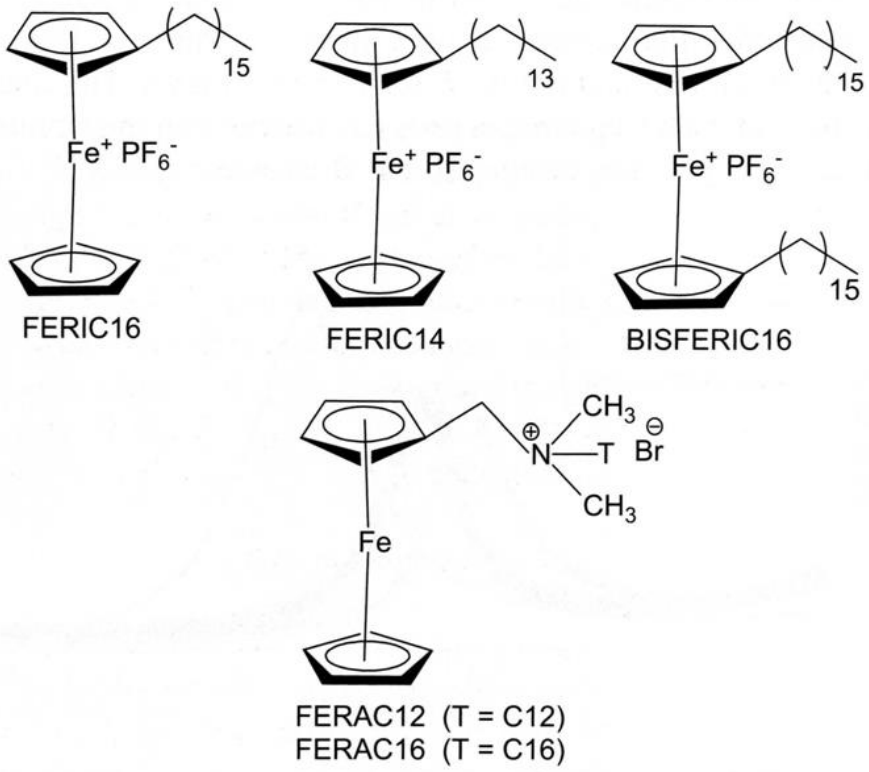

Fig. 3.: XRD traces of organically modified clays (FERAC16, FERAC12).

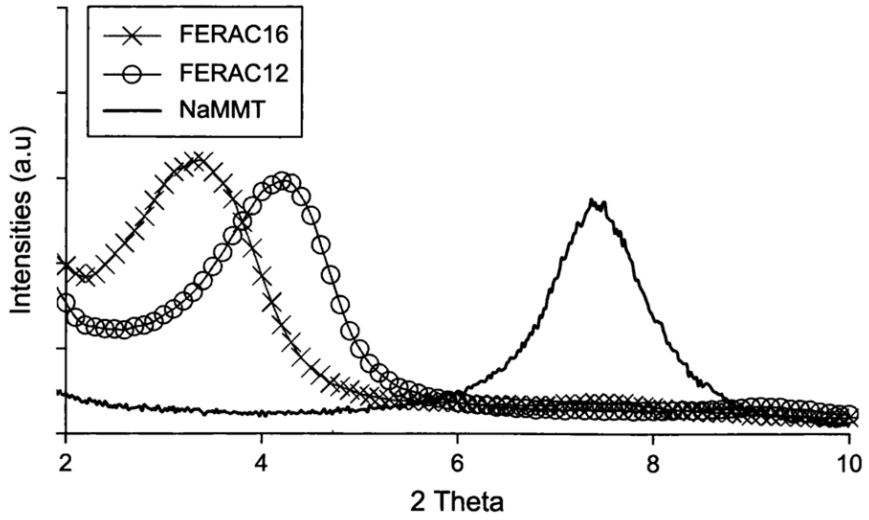

Polymer Degradation and Stability, Vol. 92, No. 10 (October 2007): pg. 1803-1812. DOI.

Fig. 4.: XRD traces of MMT and different ferrocenium modified clays, FERIC16 and BISFERIC16.

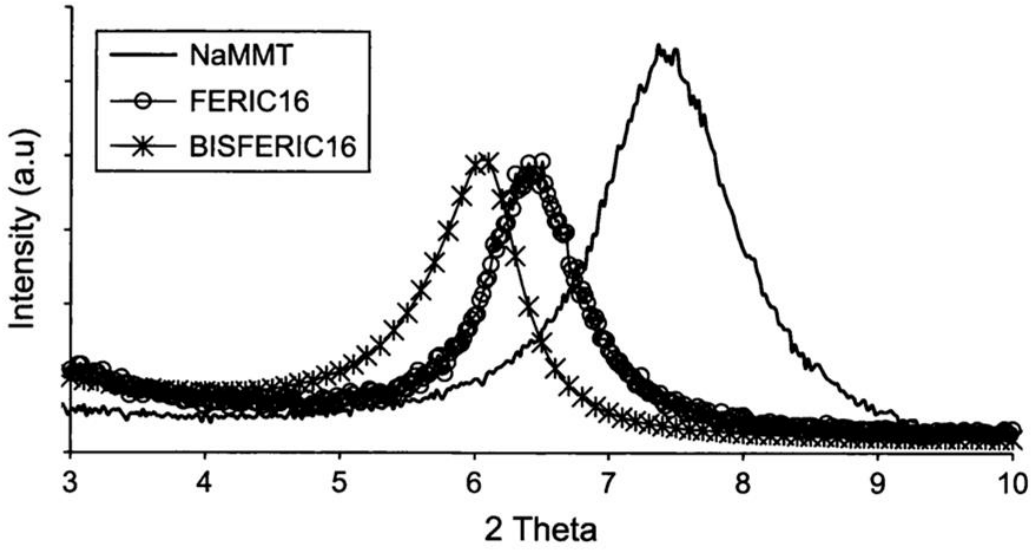

Fig. 5.: XRD traces of PS/FERAC16.

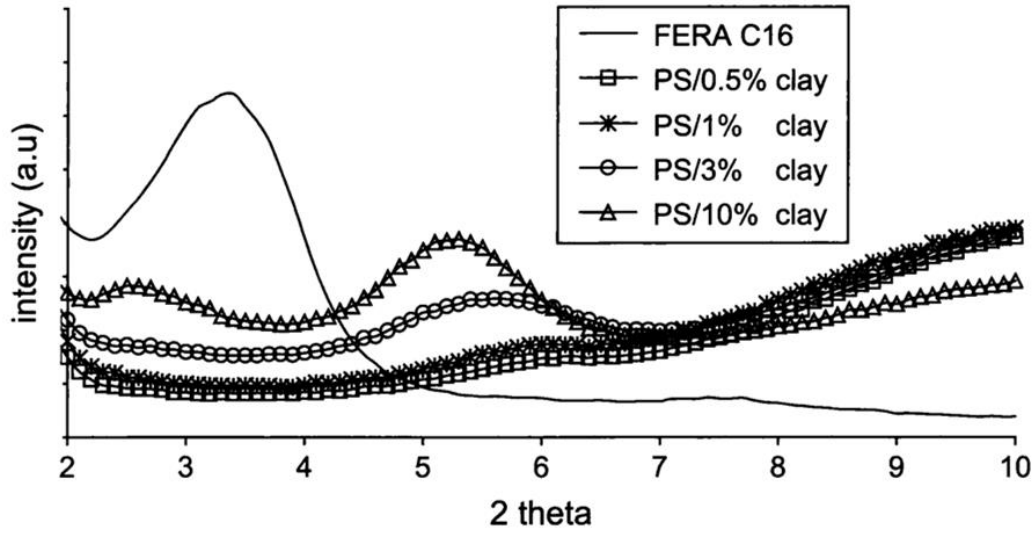

Polymer Degradation and Stability, Vol. 92, No. 10 (October 2007): pg. 1803-1812. DOI.

Fig. 6.: XRD traces of EVA/FERAC16.

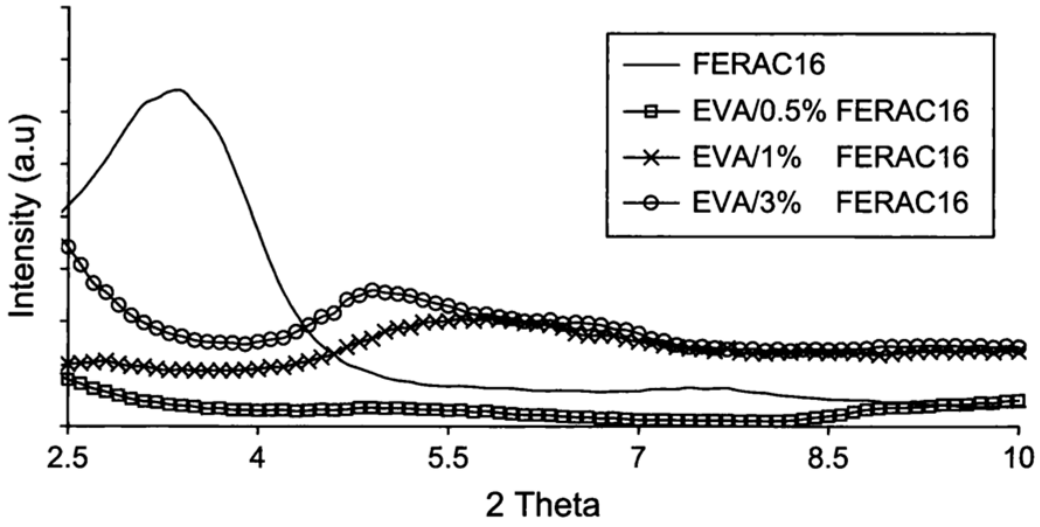

Fig. 7.: TEM images of FERAC16 in EVA and PS. On the left, the EVA/FERAC16 1% and on the right, PS/FERAC16 1%.

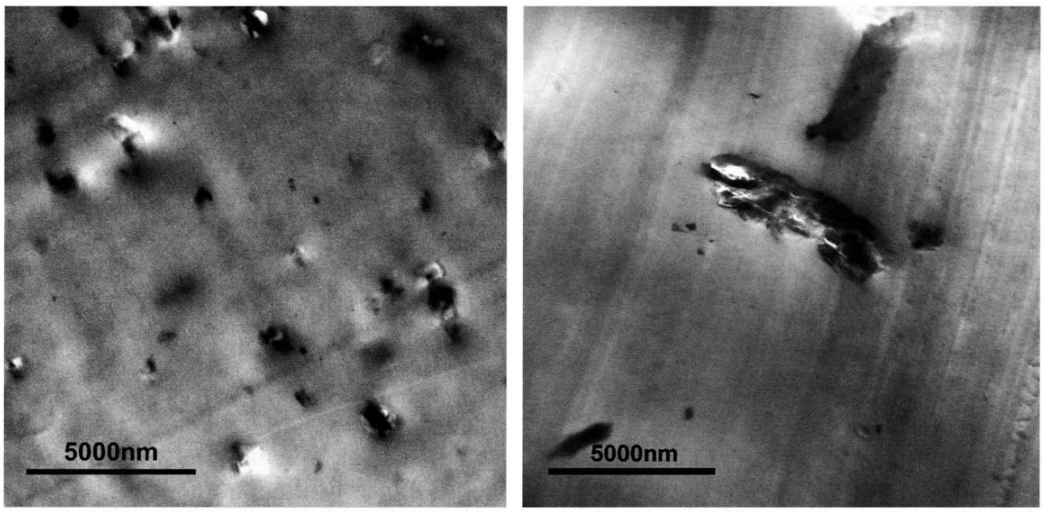

Polymer Degradation and Stability, Vol. 92, No. 10 (October 2007): pg. 1803-1812. DOI.

Fig. 8.: TEM images at low magnification. (left) PS/FERIC16 1% by melt blending and (right) PS/FERIC14 1% by melt blending.

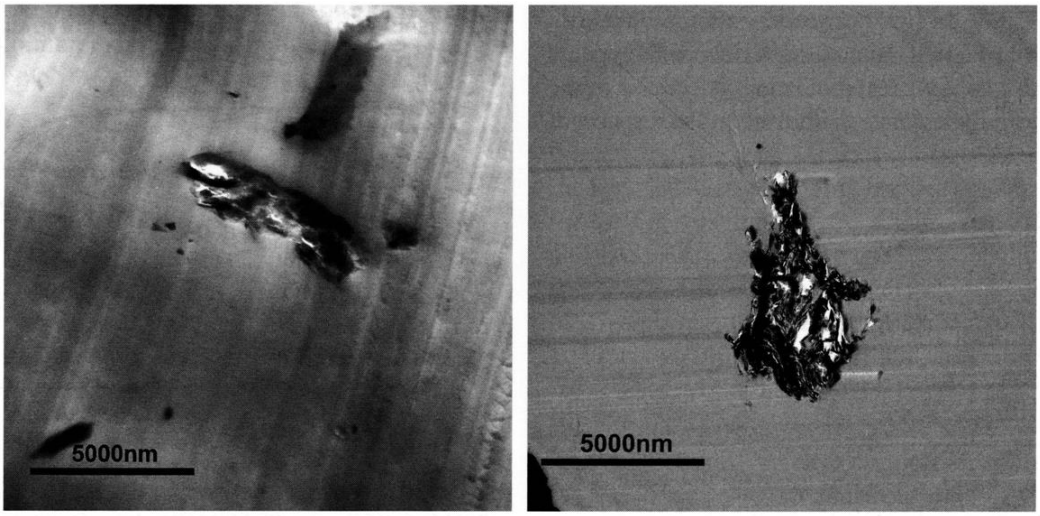

Fig. 9.: TGA Curves of FERAC12 and FERAC16 clays.

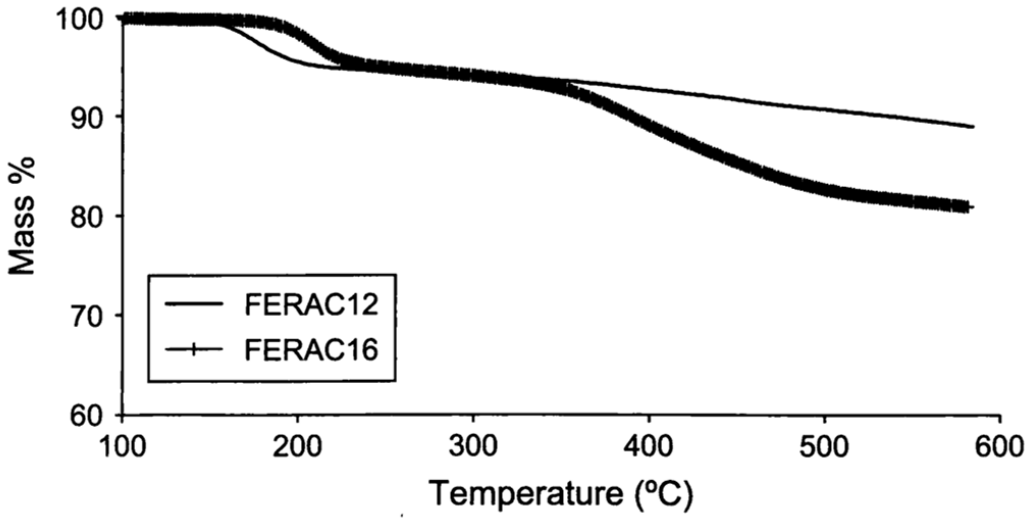

Polymer Degradation and Stability, Vol. 92, No. 10 (October 2007): pg. 1803-1812. DOI.

Fig. 10.: TGA Curves of FERIC16 and BISFERIC16 clays.

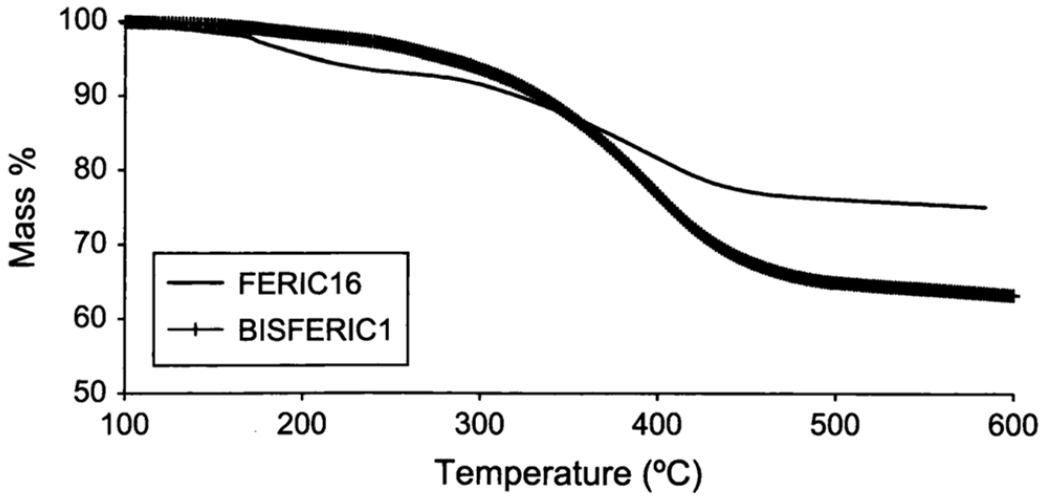

Fig. 11.: TGA profiles of (A) Pure PS and PS/FERAC16 composites; (B) PS/FERAC16 0.5%; (C) PS/FERAC16 1%; (D) PS/FERAC16 3%; (E) PS/FERAC16 5%; (F) PS/FERAC16 10%.

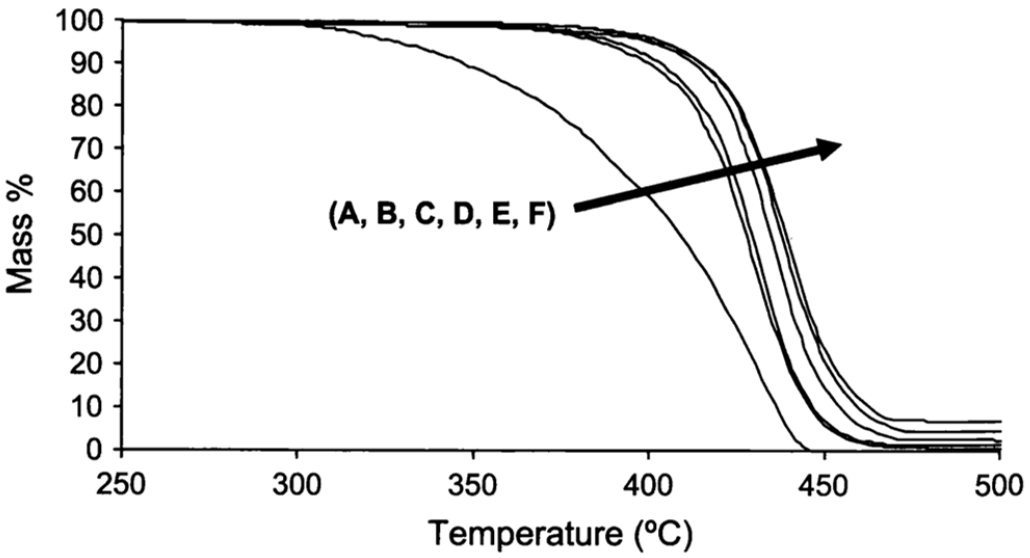

Polymer Degradation and Stability, Vol. 92, No. 10 (October 2007): pg. 1803-1812. DOI.

Fig. 12.: TGA profiles of (A) Pure PS and PS/FERIC16 composites; (B) PS/FERIC16 0.5%; (C) PS/FERIC16 1%; (D) PS/FERIC16 3%.

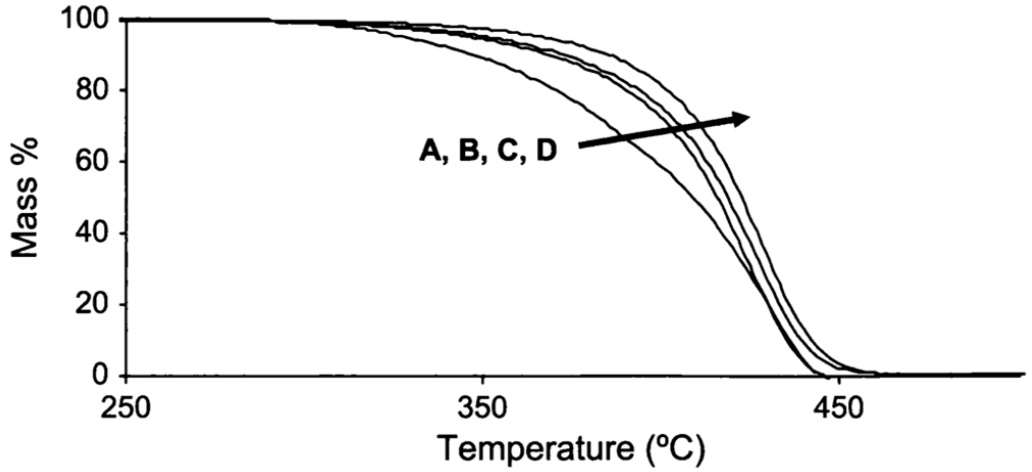

Fig. 13.: TGA profiles of (A) Pure PS and PS/BISFERIC16 composites; (B) PS/BISFERIC16 1%; (C) PS/BISFERIC16 3%; (D) PS/BISFERIC16 5%.

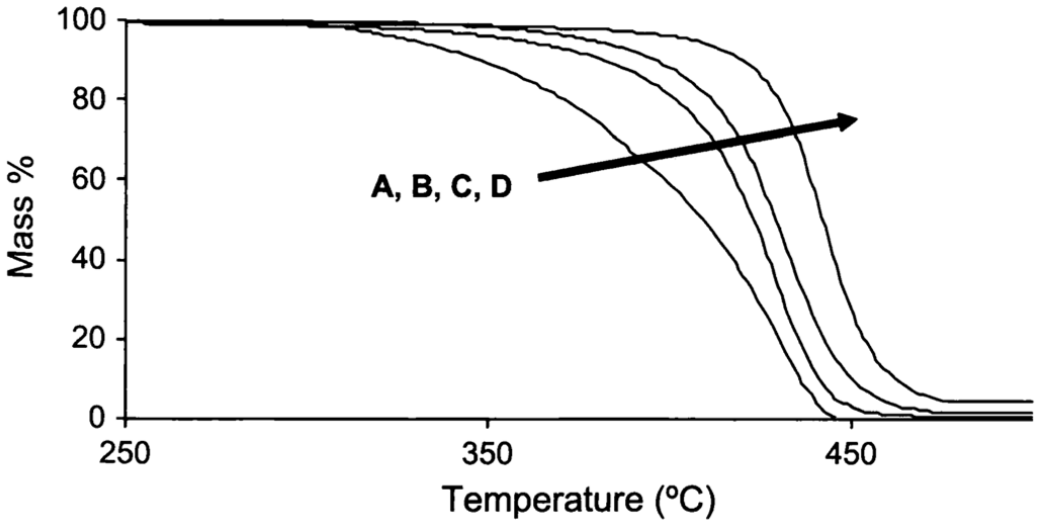

Fig. 14.: TGA profiles of (A) Pure EVA and EVA/FERAC16 composites; (B) EVA/FERAC16 0.5%; (C) EVA/FERAC16 1%; (D) EVA/FERAC16 3%.

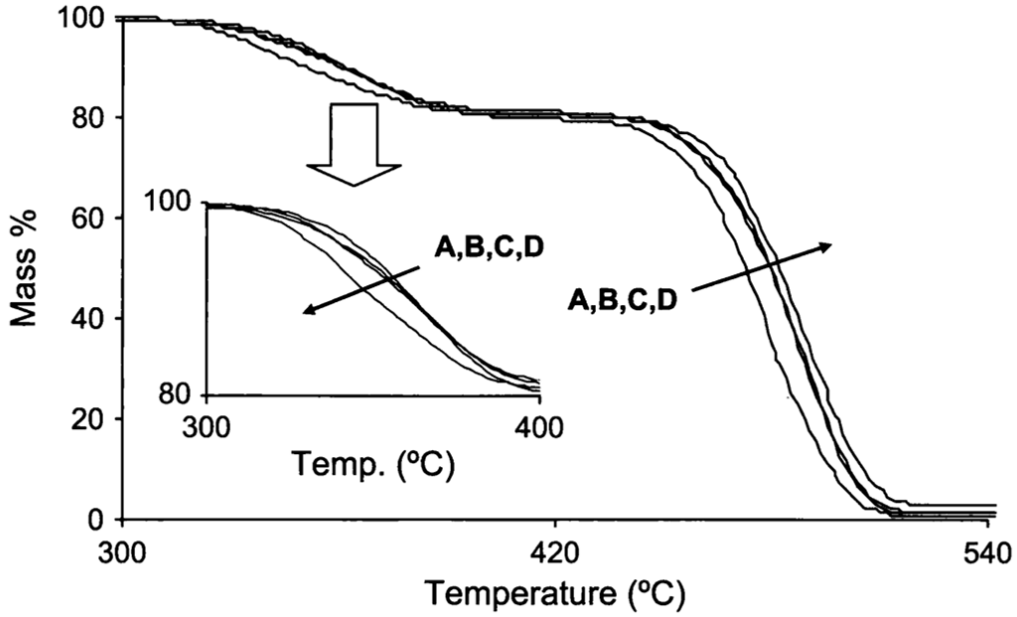

Fig. 15.: Heat release rate curves for PS and different PS/FERIC14 systems (melt blended).

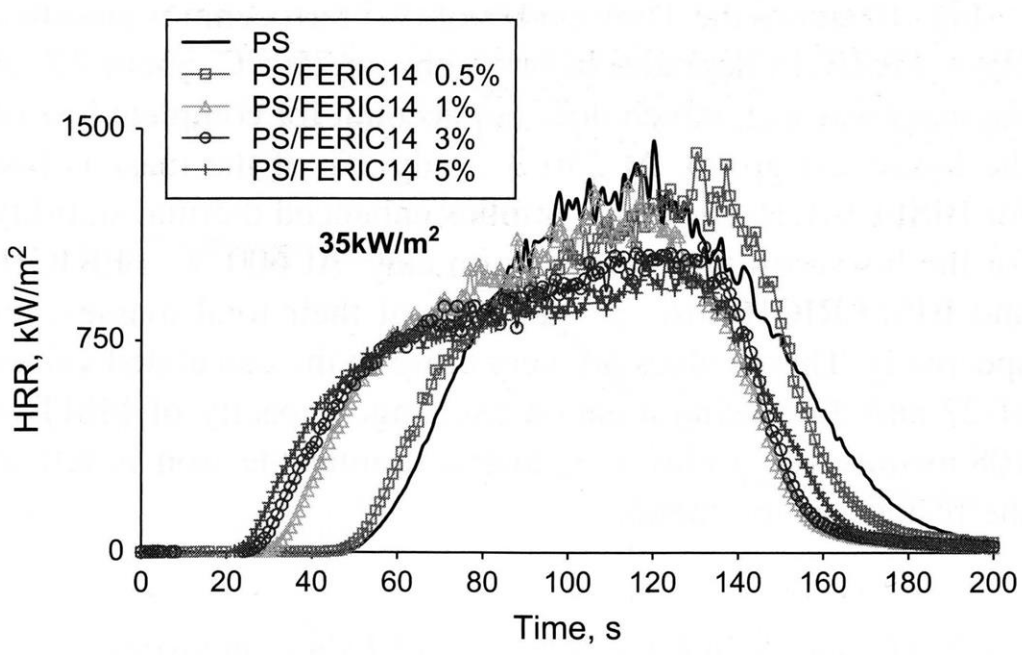

Polymer Degradation and Stability, Vol. 92, No. 10 (October 2007): pg. 1803-1812. DOI.

Fig. 16.: HRR curves of EVA and different EVA/FERAC16 systems (melt blended).